Journal of Solid State Chemistry 182 (2009) 2392–2401

Contents lists available at ScienceDirect

Journal of Solid State Chemistry

journal homepage: www.elsevier.com/locate/jssc

Organic carboxylate anions effect on the structures of a series of Mn(II) complexes based on 2-phenylimidazo[4,5-*f*]1,10-phenanthroline ligand

Xiuli Wang *, Yongqiang Chen, Guocheng Liu, Hongyan Lin, Jinxia Zhang

Faculty of Chemistry and Chemical Engineering, Bohai University, Jinzhou 121000, PR China

ARTICLE INFO

Article history:
Received 27 February 2009
Received in revised form
29 May 2009
Accepted 17 June 2009
Available online 24 June 2009

Keywords:
Hydrothermal synthesis
Crystal structure
Carboxylate anion
Manganese complexes
Properties

ABSTRACT

In our efforts to tune the structures of Mn(II) complexes by selection of organic carboxylic acid ligands, six new complexes $[Mn(PIP)_2Cl_2]$ **(1)**, $[Mn(PIP)_2(4,4'\text{-bpdc})(H_2O)]\cdot 2H_2O$ **(2)**, $[Mn(PIP)_2(1,4\text{-bdc})]$ **(3)**, $[Mn(PIP)(1,3\text{-bdc})]$ **(4)**, $[Mn(PIP)_2(2,6\text{-napdc})]\cdot H_2O$ **(5)**, and $[Mn(PIP)(1,4\text{-napdc})]\cdot H_2O$ **(6)** were obtained, where PIP = 2-phenylimidazo[4,5-*f*]1,10-phenanthroline, 4,4′-H_2bpdc = biphenyl-4,4′-dicarboxylic acid, 1,4-H_2bdc = benzene-1,4-dicarboxylic acid, 1,3-H_2bdc = benzene-1,3-dicarboxylic acid, 2,6-H_2napdc = 2,6-naphthalenedicarboxylic acid, 1,4-H_2napdc = 1,4-naphthalenedicarboxylic acid. All complexes have been structurally characterized by IR, elemental analyses, and single crystal X-ray diffraction. Structural analyses show that complexes **1** and **2** possess mononuclear structures, complexes **3**, **4**, and **5** feature chain structures, and complex **6** exhibits a 2D (4,4) network. The structural difference of **1**–**6** indicates that organic carboxylate anions play important roles in the formation of such coordination architectures. Furthermore, the thermal properties of complexes **1**–**6** and the magnetic property of **4** have been investigated.

1. Introduction

The rational design and synthesis of new discrete or polymeric transition metal-organic coordination architectures have received intense interest due to their fascinating structural topologies and potential applications as functional materials [1–7]. These coordination polymers can be specially designed by the careful selection of metal centers with preferred coordination geometries, the nature of the anions, template, the structure of the connecting ligands, and the reaction conditions [8–23]. In addition, H-bonding, π–π stacking, and host–guest interactions also affect the results, and they may further link discrete subunits or low-dimensional entities into high-dimensional supramolecular networks [24–28]. Among those mentioned above, the selection of organic carboxylate anions are extremely important because changing the structures of the anions can control and adjust the structures of coordination polymers, even for complexes containing the same secondary organic ligand and metal cation. Up to now, the effect of organic carboxylate anions on the structure formation of coordination polymers has been investigated. However, studies on Mn(II) complexes are limited in the presence of 1,10-phenanthroline derivatives [29–31].

In order to investigate the effect of the anions on the formation of Mn(II) complexes, particularly the organic carboxylate anions, we selected six structurally different organic carboxylic acids or carboxylate as the anion ligands (Chart 1). In addition, 1,10-phenanthroline (phen) has been widely used to build supramolecular architectures because of its excellent coordinating ability and large conjugated system that can easily form π–π interactions. However, far less attention has been given to their derivatives [29,32]. We previously reported on the synthesis and characterization of some complexes based on phen derivative and carboxylate anions [33–36]. As an extension of our previous work, another important phen derivative 2-phenylimidazo[4,5-*f*]1,10-phenanthroline (PIP) was used as the secondary ligand (Chart 1). Compared with 1,10-phenanthroline, this ligand contains both an extended π-system and a imidazole ring, capable of acting as hydrogen bond acceptors/donors or of forming coordination interactions to some metal ions, as well as extending the π-system themselves [37]. Hence, it is a good candidate for the construction of complexes. In contrast to the exo-bidentate dipyridyl ligands, selecting of multi-carboxylates bridge ligands are important in the terminal ligands system. Since carboxylates can connect metal ions or metal clusters into coordination polymers exhibiting intriguing structural and dimensional diversities. Thus, six organic carboxylic acid or carboxylate anion: malonate, biphenyl-4,4′-dicarboxylic acid (4,4′-H_2bpdc), benzene-1,4-dicarboxylic acid (1,4-H_2bdc), benzene-1,3-dicarboxylic acid (1,3-H_2bdc), 2,6-naphthalenedicarboxylic acid (2,6-H_2napdc) and 1,4-naphthalenedicarboxylic acid (1,4-H_2napdc) with different shape, size, and flexibility, have been used in this work. In the presence of secondary N-donor chelating ligand PIP, a series of Mn(II) complexes have been isolated: $[Mn(PIP)_2Cl_2]$ **(1)**,

* Corresponding author. Fax: +86 416 3400158.
E-mail address: wangxiuli@bhu.edu.cn (X. Wang).

0022-4596/$ - see front matter © 2009 Elsevier Inc. All rights reserved.
doi:10.1016/j.jssc.2009.06.031

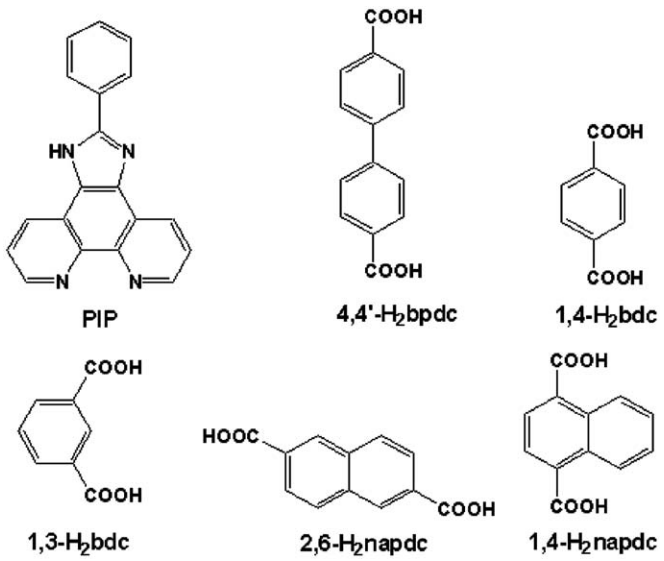

Chart 1. Ligands used in the paper.

$[Mn(PIP)_2(4,4'\text{-bpdc})(H_2O)]\cdot 2H_2O$ **(2)**, $[Mn(PIP)_2(1,4\text{-bdc})]$ **(3)**, $[Mn(PIP)(1,3\text{-bdc})]$ **(4)**, $[Mn(PIP)_2(2,6\text{-napdc})]\cdot H_2O$ **(5)**, and $[Mn(PIP)(1,4\text{-napdc})]\cdot H_2O$ **(6)**. On the basis of synthesis and structural characterization, the influence of organic carboxylate linkers on the control of the final complex structures and the role of weak intermolecular forces in the creation of molecular architectures are discussed. Moreover, thermal properties of the complexes **1**–**6** and the magnetic property of **4** have been investigated in the solid state.

2. Experimental section

2.1. Materials and instrumentation

All chemicals purchased were of reagent grade and used without further purification. PIP was synthesized by the methods of the literature [38] and characterized by FT-IR spectra and ^{1}H NMR. FT-IR spectra (KBr pellets) were taken on a Magna FT-IR 560 spectrometer. Elemental analyses (C, H, and N) were performed on a Perkin-Elmer 240C analyzer. Thermogravimetric data for the complexes **1**–**6** were collected on a Pyris Diamond thermal analyzer. Fluorescence spectra were performed on a Hitachi F-4500 fluorescence/phosphorescence spectrophotometer at room temperature. Powder X-ray diffraction (PXRD) data were collected on a Bruker D8-ADVANCE diffractometer equipped with Cu$K\alpha$ at a scan speed of 1° min^{-1}. Magnetic susceptibility measurement for **4** was carried out using a Quantum Design MPMS XL-5 SQUID magnetometer at field of 1000 Oe. Diamagnetic correction was estimated from Pascal's constants [39].

2.2. Synthesis

2.2.1. $[Mn(PIP)_2Cl_2]$ (**1**)

A mixture of $MnCl_2\cdot 4H_2O$ (0.1 mmol), PIP (0.1 mmol), $CH_2(COONa)_2$ (0.1 mmol), and H_2O (10 ml), stirred for 20 min, was sealed to a Teflon-lined stainless steel autoclave (25 ml) and kept at 180 °C for 3 days. After the mixture was slowly cooled to room temperature, yellow block crystals suitable for X-ray diffraction of complex **1** were obtained in 38% yield (based on Mn). IR (KBr pellet, cm^{-1}): 3060w, 2360m, 1608w, 1581s, 1477m 1386s, 1338m, 1213s, 1128m, 1080s, 823m, 732m. Anal. Calcd. for $C_{38}H_{24}Cl_2MnN_8$: C 63.50; H 3.34; N 15.60%. Found: C 63.65; H 3.19; N 15.49%.

2.2.2. $[Mn(PIP)_2(4,4'\text{-bpdc})(H_2O)]\cdot 2H_2O$ (**2**)

A mixture of $Mn(CH_3COO)_2\cdot 4H_2O$ (0.1 mmol), PIP (0.05 mmol), biphenyl-4,4′-dicarboxylic acid (0.05 mmol), NaOH (0.12 mmol), and H_2O (8 ml), stirred for 20 min, was sealed to a Teflon-lined stainless steel autoclave (25 ml) and kept at 160 °C for 5 days. After the mixture was slowly cooled to room temperature, yellow block crystals suitable for X-ray diffraction of complex **2** were obtained in 30% yield (based on Mn). IR (KBr pellet, cm^{-1}): 3425w, 3062w, 2362m, 1570s, 1460m, 1386s, 1070m, 947m, 821w, 731m. Anal. Calcd. for $C_{52}H_{30}MnN_8O_7$: C 65.88; H 2.22; N 12.00%. Found: C 65.71; H 2.02; N 12.19%.

2.2.3. $[Mn(PIP)_2(1,4\text{-bdc})]$ (**3**)

3 was obtained by the similar method to that for **2**, excepted for using benzene-1,4-dicarboxylic acid (16.6 mg, 0.1 mmol) instead of biphenyl-4,4′-dicarboxylic acid and NaOH (0.12 mmol). Yield: 25% (based on Mn). IR (KBr pellet, cm^{-1}): 3421w, 3062w, 2360m, 1568s, 1458s, 1386s, 1070m, 948m, 821m, 786m. Anal. Calcd. for $C_{46}H_{26}MnN_8O_4$: C 68.23; H 3.21; N 13.24%. Found: C 68.39; H 3.11; N 13.10%.

2.2.4. $[Mn(PIP)(1,3\text{-bdc})]$ (**4**)

4 was obtained by the similar method to that for **3**, excepted for using benzene-1,3-dicarboxylic acid instead of benzene-1,4-dicarboxylic acid. Yield: 30% (based on Mn). IR (KBr pellet, cm^{-1}): 342w, 3061w, 2360m, 1572s, 1460s, 1358s, 1072m, 831m, 732m. Anal. Calcd. for $C_{27}H_{16}MnN_4O_4$: C 62.91; H 3.05; N 10.87%. Found: C 62.74; H 2.82; N 11.01%.

2.2.5. $[Mn(PIP)_2(2,6\text{-napdc})]\cdot H_2O$ (**5**)

5 was obtained by the similar method to that for **1**, excepted for using 2,6-naphthalenedicarboxylic acid instead of $CH_2(COONa)_2$, $MnSO_4$ instead of $MnCl_2$ and NaOH (0.32 mmol). Yield: 28% (based on Mn). IR (KBr pellet, cm^{-1}): 3504m, 3066w, 2362m, 1772w, 1570s, 1400s, 1074m, 958w, 829w, 734m, 702m, 680w. Anal. Calcd. for $C_{50}H_{30}MnN_8O_5$: C 68.42; H 3.42; N 12.77%. Found: C 68.23; H 3.56; N 12.59%.

2.2.6. $[Mn(PIP)(1,4\text{-napdc})]\cdot H_2O$ (**6**)

A mixture of $Mn(NO_3)_2\cdot 6H_2O$ (0.2 mmol), PIP (0.05 mmol), 1,4-naphthalenedicarboxylic acid (0.2 mmol), NaOH (0.41 mmol), and H_2O (8 ml), stirred for 20 min, was sealed to a Teflon-lined stainless steel autoclave (25 ml) and kept at 160 °C for 5 days. After the mixture was slowly cooled to room temperature, yellow block crystals suitable for X-ray diffraction of complex **6** were obtained in 20% yield (based on Mn). IR (KBr pellet, cm^{-1}): 3504w, 3215w, 2360m, 1571s, 1458s, 1357s, 1074m, 835m, 732m, 580w. Anal. Calcd. for $C_{31}H_{18}MnN_4O_5$: C 64.03; H 3.10; N 13.77%. Found: C 64.18; H 2.97; N 13.84%.

2.3. X-ray crystallographic measurements

All diffraction data were collected using a Bruker Apex CCD diffractometer (Mo$K\alpha$ radiation, graphite monochromator, $\lambda = 0.71073$ Å). The structures were solved by direct methods with *SHELXS-97* and Fourier techniques and refined by the full-matrix least-squares method on F^2 with *SHELXL-97* [40,41]. All non-hydrogen atoms were refined anisotropically, and hydrogen atoms of the ligands were generated theoretically onto the specific atoms and refined isotropically with fixed thermal factors, and the H atoms of water molecules were located in different Fourier

Table 1
Crystal data and structure refinement parameters for complexes **1**–**6**.

Complex	1	2	3
Formula	$C_{38}H_{24}Cl_2MnN_8$	$C_{52}H_{34}MnN_8O_7$	$C_{46}H_{28}MnN_8O_4$
Fw	718.49	937.81	811.70
Crystal system	Orthorhombic	Orthorhombic	Triclinic
Space group	*Pnna*	$Pna2_1$	$P-1$
a (Å)	8.6553(5)	17.5733(17)	9.674(2)
b (Å)	28.2681(18)	15.7815(15)	10.464(2)
c (Å)	15.2024(10)	16.4858(16)	10.670(3)
α (deg)	90	90	90.52(4)
β (deg)	90	90	115.38(3)
γ (deg)	90	90	111.47(3)
V (Å^3)	3719.6(4)	4572.1(8)	890.3(4)
D (g cm^{-3})	1.283	1.362	1.514
Z	4	4	1
F(000)	1372	1932	417
μ (mm^{-1})	0.536	0.352	0.433
Tot. data	16 989	22 565	4527
Uniq. data	3170	8118	3078
R_{int}	0.0423	0.0838	0.0375
R^a/wR^b	0.0652/0.1483	0.0848/0.1878	0.0597/0.1095
GOF on F^2	1.040	0.976	0.991
Complex	4	5	6
Formula	$C_{27}H_{16}MnN_4O_4$	$C_{50}H_{30}MnN_8O_5$	$C_{31}H_{18}MnN_4O_5$
Fw	515.38	877.76	581.43
Crystal system	Monoclinic	Monoclinic	Monoclinic
Space group	*C*2/*c*	*P*2/*n*	*P*21/*c*
a (Å)	15.3556(9)	12.716(2)	12.2521(12)
b (Å)	15.9303(9)	11.6747(18)	15.1778(15)
c (Å)	18.8663(14)	14.079(2)	16.9597(12)
α (deg)	90	90	90
β (deg)	109.37(1)	90.754(3)	127.606(5)
γ (deg)	90	90	90
V (Å^3)	4353.7(5)	2089.8(6)	2498.5(4)
D (g cm^{-3})	1.573	1.395	1.546
Z	8	2	4
F(000)	2104	902	1188
μ (mm^{-1})	0.652	0.376	0.581
Tot. data	13 393	10 538	9499
Uniq. data	5115	3699	3034
R_{int}	0.0303	0.0671	0.0353
R^a/wR^b	0.0375/0.0842	0.0535/0.0913	0.0341/0.0790
GOF on F^2	1.012	1.058	1.012

[a] $R = \Sigma(||F_o|-|F_c||)/\Sigma|F_o|$.
[b] $wR2 = [\Sigma w(|F_o|^2-|F_c|^2)^2/(\Sigma w|F_o|^2)^2]^{1/2}$.

synthesis maps. All the crystal data and structure refinement details for the six complexes are given in Table 1. The data of relevant bond distances and angles are listed in Table S1, and hydrogen-bonding geometries are summarized in Table S2. Crystallographic data for the structures reported in this paper have been deposited in the Cambridge Crystallographic Data Center with CCDC reference numbers 715046–715051 for compounds **1**–**6**, respectively.

3. Results and discussion

3.1. Structure descriptions of complexes 1−6

3.1.1. [Mn(PIP)$_2$Cl$_2$] (1)

The structure of **1** consists of two PIP ligands, two chlorine anions and a Mn(II) cation. The perspective view of **1** is shown in Fig. 1a, and the selected bond distances and angles are listed in Table S1. The Mn(II) ion was coordinated in a distorted octahedral geometry by four nitrogen atoms of two PIP ligands with normal Mn–N distances from 2.300(3) to 2.304(3) Å, and two chlorine anions with the Mn–Cl distance is 2.506(1) Å. The adjacent discrete mononuclears are arranged into a 3D supramolecular architecture by inter-molecular π–π interactions (Fig. S1). The face-to-face distances between PIP ligands are from 3.551 to 3.591 Å (the dihedral angle is 1.02°, 1.49°, and 2.20°, respectively). Moreover, the open supramolecular framework has channels with the estimated solvent-accessible void volume, which is 21.6% of the total crystal volume, as shown in Fig. 1b. Interestingly, $CH_2(COONa)_2$ plays a key role in the formation of **1**. All our attempts to separate complex **1** into good-quality for X-ray analysis have been thus far unsuccessful without the presence of $CH_2(COONa)_2$.

3.1.2. [Mn(PIP)$_2$(4,4′-bpdc)(H$_2$O)]·2H$_2$O (2)

Complex **2** has similar neutral coordination environment to that of **1**, also showing distorted octahedral geometry (see Fig. 2a). Each Mn(II) ion was coordinated by four nitrogen atoms from PIP ligands and two oxygen atoms from 4,4′-bpdc and one water molecule, respectively, [Mn(1)–N = 2.272(6)–2.345(6) Å, Mn(1)–O = 2.114(6)–2.187(6) Å]. Moreover, there are two disordered uncoordinated water molecules in **2**, which can link hydrogen bond acceptor by weak interactions to stabilize the structure of complex **2**. In complex **2**, the PIP ligand plays an important role in the formation of a 1D infinite zigzag supramolecular chain by π–π stacking interactions (see Fig. 2b). The face-to-face distance between the paired PIP rings is about 3.629(5) Å.

3.1.3. [Mn(PIP)$_2$(1,4-bdc)] (3)

Complex **3** forms a 1D polymeric chain. As shown in Fig. 3a, the Mn(II) ion features a distorted octahedral geometry, coordinated by four nitrogen atoms from two PIP ligands with the Mn(1)–N distances of 2.298(4)–2.319(4) Å, and two oxygen atoms from two different 1,4-bdc ligands [Mn(1)–O = 2.114(3) Å]. In **3,** the 1,4-bdc ligands only assume a kind of coordination mode, namely, bridging bis(monodentate). The adjacent Mn(II) ions are bridged by 1,4-bdc ligands to form a 1D linear chain with the distance of Mn–Mn is 11.357 Å. Compared with those of **1** and **2**, the arranged fashion of the PIP ligands in **3** is different, leading to a structure suitable to form π–π interactions. Thus, the lateral PIP ligands from adjacent 1D chains are paired to furnish π–π interactions resulting in 2D supramolecular layer (Fig. 3b). The face-to-face distance between the paired PIP rings is 3.744(4) Å (the dihedral angle is 14.27°). In fact, π–π stacking interactions play an important role in the formation and stabilization of the supramolecular structure [29]. In addition, the 2D supramolecular layers are further extended into a 3D supramolecular framework (Fig. 3c) through hydrogen bonds [the distance N(4)–H(4B)···O(2) of 2.780(5) Å]. Thus, the weak noncovalent interactions are important in the formation of the final supramolecular structure of **3**. It is noteworthy that the structure of **3** is entirely different from that of the related complex [Mn(1,4-bdc)(phen)] [42], which possesses a dinuclear [Mn$_2$(phen)$_2$(1,4-bdc)$_4$] building block bridged by two μ-carboxylate to form a 3D structure. The result is probably due to the larger steric hindrance of PIP ligand.

3.1.4. [Mn(PIP)(1,3-bdc)] (4)

To investigate the influence of the spacer of ligand (the position of carboxyl group) on the structure of complex, 1,3-H$_2$bdc ligand instead of 1,4-H$_2$bdc ligand was used, and a new complex **4** was obtained and structurally determined. The coordination environment of complex **4** consists of two Mn(II) ions [Mn(1), Mn(1A)], four nitrogen atoms from two PIP ligands and eight oxygen atoms from different 1,3-bdc ligands (Fig. 4a).

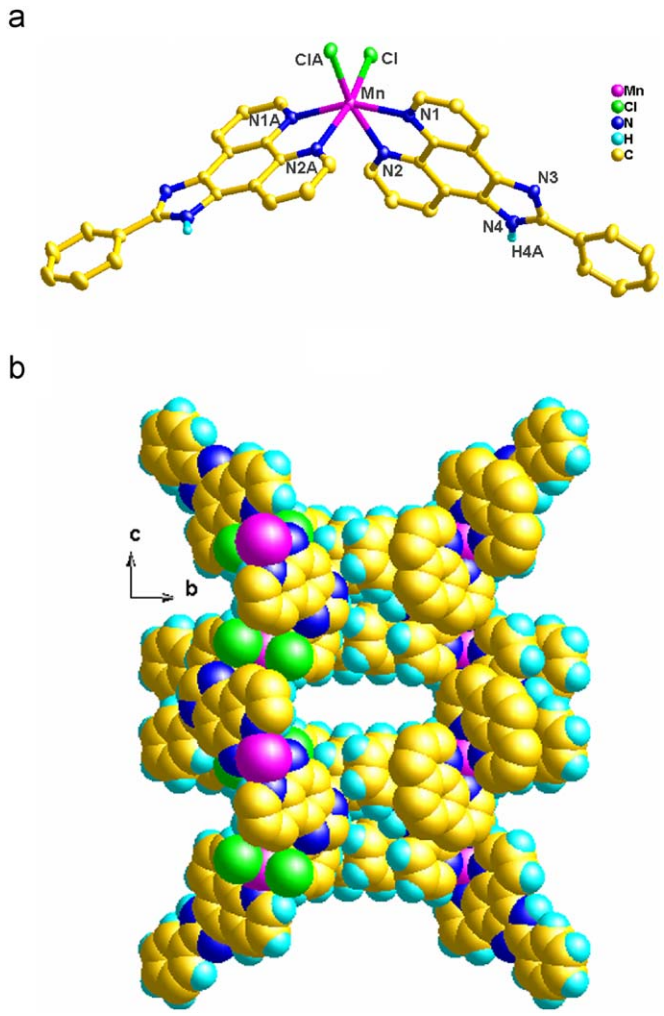

Fig. 1. View of (a) the coordination environment of Mn(II) in **1** (symmetry code: **A**: $x,-y-1/2,-z+1/2$); (b) space-filling diagram of the packing down the a–axis in **1**, showing the rectangular channels.

Each Mn(II) ion is located in a distorted octahedral geometry, with Mn–N distances from 2.276(2) to 2.308(2) Å, and Mn–O distances varying from 2.122(1) to 2.342(2) Å, respectively. It was noted that the coordination environment of the Mn(II) ion is clearly different from complexes **1**–**3,** probably as a result of steric arrangement from the aromatic dicarboxylate groups. Two carboxylate groups of 1,3-bdc ligands adopted bridging bidentate and chelating bidentate coordination modes linking dinuclear Mn_2 units [Mn(1)···Mn(1A) = 4.081 Å] to form a unique ribbon chain structure along the c-axis (Fig. S2). Interestingly, the PIP ligands are alternately attached to both sides of the ribbon chain improving stabilization by π–π interactions of intra-molecule. Furthermore, all the chains are extended by hydrogen-bonding [N(4)–H(4A)···O(4), 2.855(2) Å] into a 3D supramolecular network (Fig. 4b).

3.1.5. *[Mn(PIP)$_2$(2,6-napdc)]·H$_2$O* (**5**)

To evaluate the effect of two phenyl groups of the dicarboxylate ligand on the framework formation of complex, we selected 2,6-H_2napdc to react with manganese salt and obtained complex **5**. In **5,** each Mn(II) ion was linked by two oxygen atoms of carboxylate and four nitrogen atoms of PIP (Fig. 5a). The overall geometry is best described as a distorted octahedral geometry with the distance of Mn–O 2.136(2) Å, and Mn–N from 2.323(3) to 2.377(3) Å. Furthermore, there exists an uncoordinated guest water molecule for **5.** The adjacent Mn(II) ions are linked by 2,6-napdc of which the two carboxyl groups all adopt bridging bis(monodentate) coordination mode to form 1D zigzag chains along the c-axis (Fig. S3). Moreover, the adjacent 1D zigzag chains are further extended into a 3D supramolecular architecture by inter-molecular hydrogen bond interactions [N(4)–H(4A)···O(1) = 2.724(5) Å] (Fig. 5b).

3.1.6. *[Mn(PIP)(1,4-napdc)]·H$_2$O* (**6**)

Complex **6**, obtained by using 1,4-H_2napdc, exhibits a 2D (4,4) grid by dinuclear Mn_2 units with the Mn(1)···Mn(1A) distance is 4.970 Å (see Fig. 6b). Fig. 6a illustrates the coordination environments of the Mn(II) ions. Each Mn(II) ion was coordinated by four carboxylic oxygen atoms of two different 1,4-napdc ligands (Mn–O = 2.124(2)–2.237(2) Å, which are close to those of $[Mn(1,4\text{-napdc})]_n$ with the Mn–O distances are in the range of 2.110(2)–2.260(2) Å [43]), and two nitrogen atoms from PIP ligand with normal Mn–N distances [from 2.224(2) to 2.295(3) Å]. Moreover, there exists one lattice water molecule, which itself acting as a hydrogen bond donor to oxygen atom of carboxylic groups to form intra-molecular hydrogen bond stabilized the structure of **6**. The dinuclear Mn_2 units are linked by 1,4-napdc of which the two carboxyl groups adopt different coordination models [bridging mono(bidentate) and chelating mono(bidentate)] to form 2D network. The coordination model of 1,4-napdc is different from that of the related complex $[Mn(1,4\text{-napdc})]_n$ [43]. The difference is probably related to the extended π-system of PIP ligand. It is noteworthy that there are different types of π–π interactions compared with those of complexes **1**–**5**. The neighboring 2D layers interacted by π–π stacking interactions between the PIP and 1,4-napdc ligands [face-to-face distances ca. 3.478(2) and 3.696(2) Å], leading to a 3D supramolecular structure (Fig. S4).

3.2. *Effect of organic carboxylate anions and PIP ligand on the structures of the complexes*

By selecting the different organic carboxylate ligands under hydrothermal condition, six new Mn(II) complexes have been successfully obtained. Although both the phen and PIP molecules are planar, there is an additional phenyl group present in the PIP ligand. The bulky phenyl group in the backbone may significantly increase the steric hindrance of the PIP ligand, leading to structural differences in their complexes [44]. In complexes **1** and **2**, the π–π interactions of the PIP ligands in them are similar. The discrete molecules interact through π–π interactions between the PIP ligands to form 3D open supramolecular framework and 1D infinite zigzag supramolecular chains, respectively. Although complexes **3**–**5** all show chain structures, the weak interactions of the PIP ligands in them are slightly different. In **3**, the linear chains interact through π–π interactions between the PIP ligands to form 2D supramolecular layer. Furthermore, H-bonding interaction extends the structure into 3D supramolecular structure. However, the π–π interactions do not play a critical role in complexes **4** and **5**, the supramolecular architectures assembled via H-bonding interactions. For **6**, there are two types of π–π interactions (one type of π–π interaction between the PIP ligands, another type of π–π interaction between the PIP and 1,4-napdc ligands), the adjacent 2D layers were arranged to 3D supramolecular structure via π–π interactions.

Generally, the role of organic carboxylate ligands can be illustrated in terms of their differences in shape, size, and

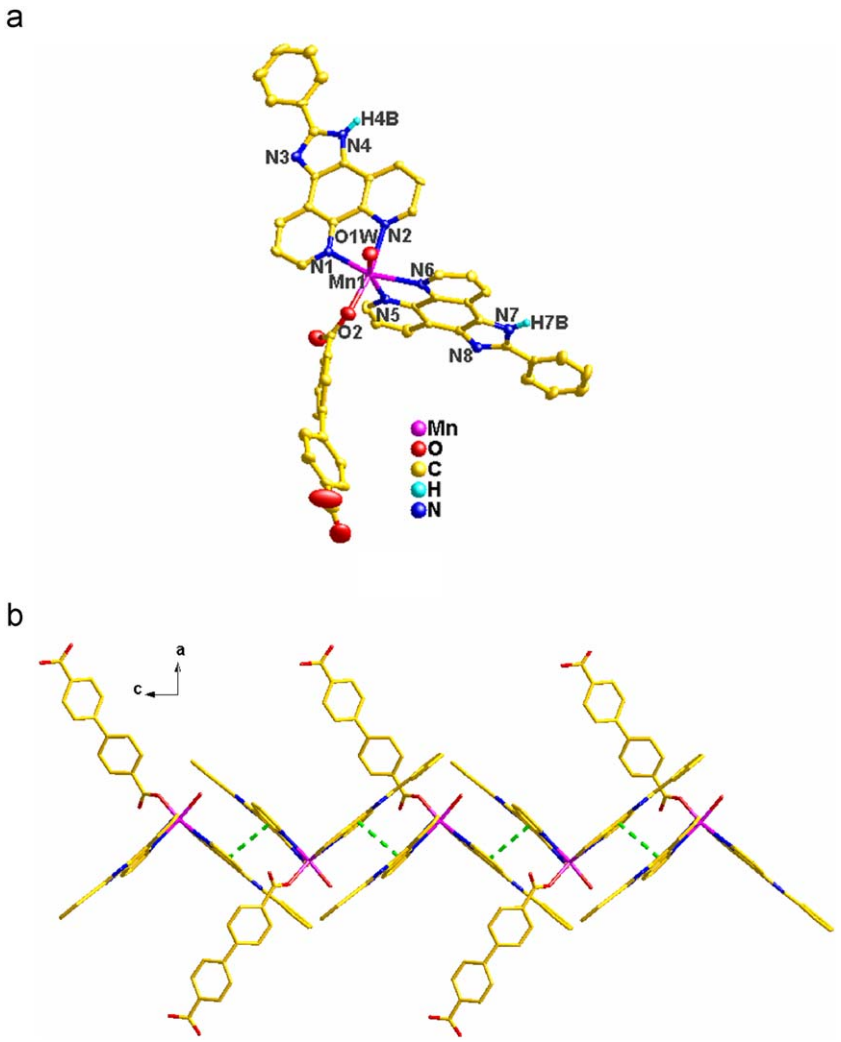

Fig. 2. View of (a) the coordination environment of Mn(II) in **2**; (b) the 1D chain formed through π–π weak interactions.

flexibility. To date, metal Pb(II) complexes based on organic acids and PIP mixed ligands have been prepared and characterized by Ma and co-workers, where illustrating that the organic acids and neutral chelating ligands have important influences on the structures of complexes [32,44]. In this work, to investigate the influence of the flexibility of organic carboxylate on the structures of metal Mn(II) complexes, we selected malonate anion as organic carboxylate ligand. Unfortunately, malonate anion cannot coordinate to Mn(II) ion in **1**, as shown in Fig. 1a. However, all our attempts to separate complex **1** into good-quality for X-ray analysis have been thus far unsuccessful in the absence of malonate anion. Because the hydrothermal reaction takes place in a sealed vessel in certain conditions, it is very difficult to assess the role of each of the reagents used. However, as is the case in the results reported here, some reagents may control the formation of the product in ways that are difficult to predict beforehand [45]. For **2**, the rigid-rod tether 4,4′-H_2bpdc was employed, intending to observe the effect of long rigid ligand on the assembly of complexes. However, the expected dimension was not obtained in **2**. In addition, the effect of aromatic carboxylate ligands with different shape and size on the structures of complexes is also revealed by the structural differences of **3**–**6**. In contrast with 1,4-H_2bdc, 1,3-H_2bdc, 2,6-H_2napdc, and 1,4-H_2napdc, the common feature of the four ligands is that each contains two carboxyl groups. However, 2,6-H_2napdc and 1,4-H_2napdc have larger conjugated π-system from the additional benzene ring. In contrast, the 1,4-bdc and 1,3-bdc ligands possess different steric hindrance. The two carboxylate groups have 180° and 120° angles, respectively. 1,4-bdc is very rigid and the two carboxyl groups adopt bridging bis(monodentate) coordination mode, which resulted a 1D linear chain in **3**. Different from 1,4-bdc, the carboxyl groups of 1,3-H_2bdc are at 1,3-positions, which are convenient bridging units for linking the adjacent metallic clusters, and bridge two adjacent metal ions to form a 1D ribbon chain in **4**. It is noted that complex **4** has dinuclear Mn_2 repeating units. Thus, it is clear that the shape of aromatic dicarboxylate ligands (the position of carboxyl group) is an important factor during the formation of complexes. We select 2,6-H_2napdc and 1,4-H_2napdc, intending to observe the size effect on the assembly of the structures in **5** and **6**. Furthermore, the rodlike napdc possess interesting features that are conducive to the formation of versatile coordination structures [46]. As can be seen in complex **5**, two carboxyl groups of the 2,6-napdc ligand bridge Mn(II) ion, which is similar to that of complex **3**, whereas the different 1D chains structure was observed in **5**. Complexes **4** and **5** show different 1D chain structures, and

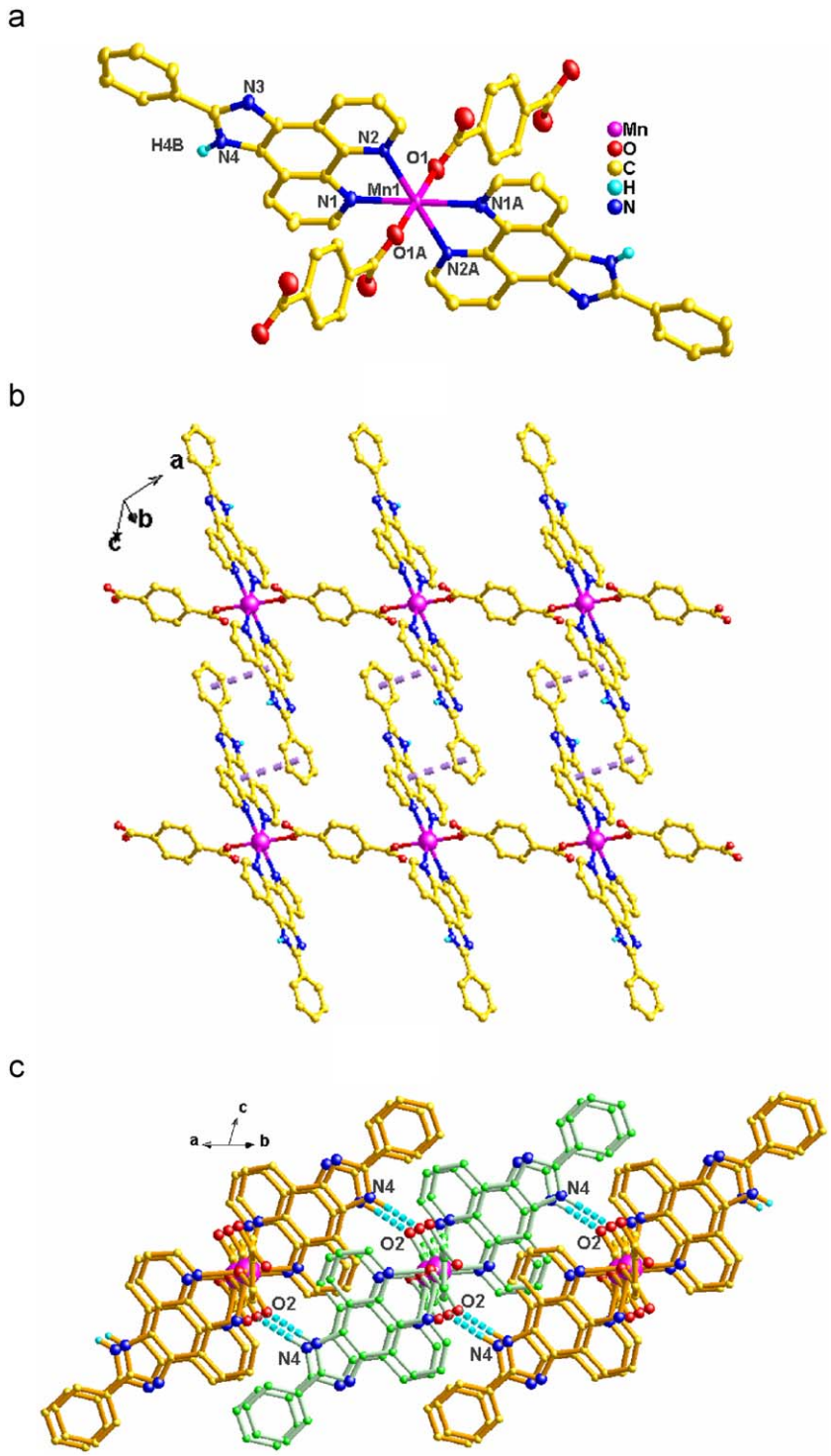

Fig. 3. View of (a) the coordination environment of Mn(II) in **3** (symmetry code: **A**: $-x+2$, $-y+2$, $-z+1$); (b) the 2D supramolecular structure formed between 1D chains by π–π weak interactions; (c) stacking of the 2D supramolecular network leading to the 3D structure by hydrogen-bonding interactions.

the chains recognize each other under the direction of hydrogen bond interactions to give 3D supramolecular structures. It should be noted that the 2D layer framework was obtained in complex **6**. Like that of complexes **3** and **4**, the influence of carboxylate positions on the complex structures is also demonstrated by the structural differences of **5** and **6**. Compared with 1,4-bdc, the 1,4-napdc ligands possess an additional benzene ring. Meanwhile, the planar 1,4-napdc anion has a conjugated π-electron system. These features allow the 1,4-napdc ligand have more chance to assemble the higher dimensional complex in presence of PIP ligand. Obviously, as far as complexes **1**–**6** are concerned, the organic carboxylate ligands are the most critical factors in determining the final structures of the coordination complexes.

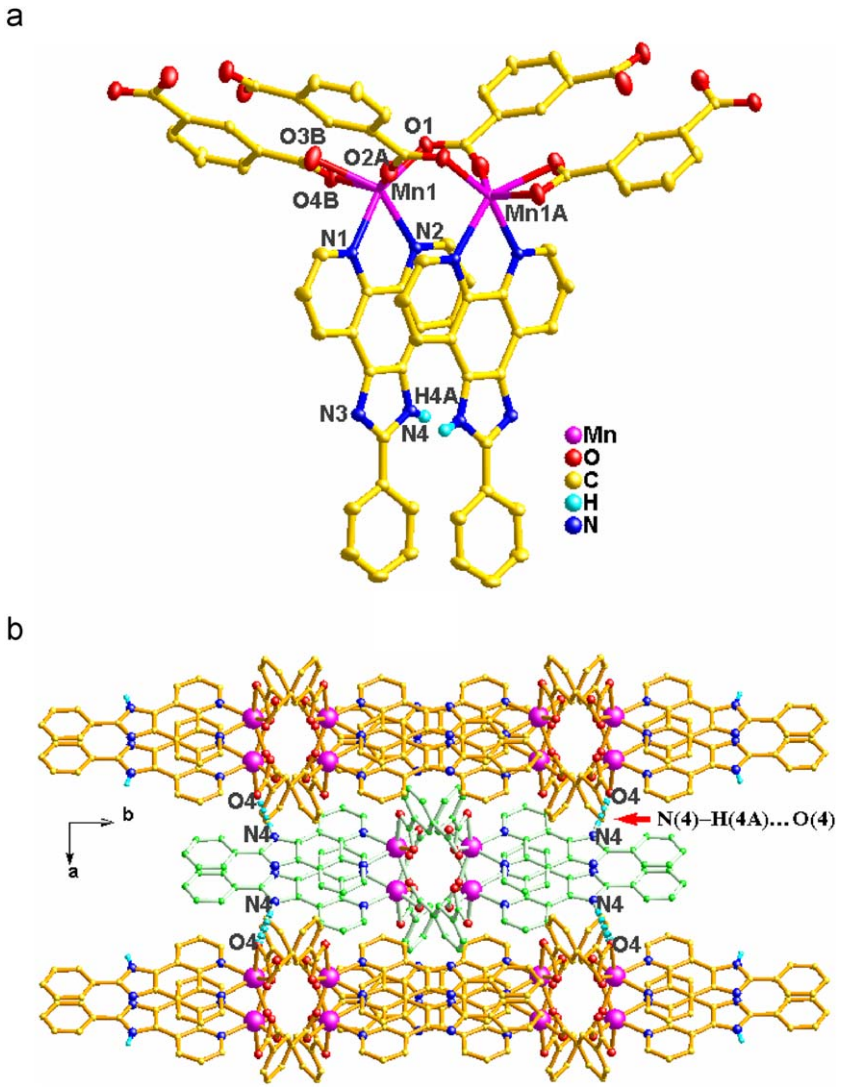

Fig. 4. View of (a) the coordination environment of Mn(II) in **4** (symmetry code: **A**: $-x$, y, $-z+1/2$; **B**: x, $-y+1$, $z-1/2$); (b) the 3D network formed by N–H···O weak interactions between 1D ribbon chains along the *c*-axis.

3.3. *Powder X-ray diffractions and thermal properties of complexes* **1**−**6**

Figs. S5–10 (supporting information) present the powder X-ray diffraction patterns for complexes **1**–**6**. The PXRD patterns of all complexes are in good agreement with their corresponding simulated patterns, indicating phase purities of these samples. The difference in reflection intensities between the simulated and the experimental patterns is due to the different orientation of the crystals in the powder samples [47].

In order to investigate thermal stability of the bulk materials, thermogravimetric analysis (TGA) was carried out for **1**–**6** (Fig. S11). The TGA curve of **1** showed that it was stable up to 311 °C and began to decompose upon heating up to about 510 °C, giving a weight loss of about 17.68%, which is consistent with the removal of organic ligands (calcd. 17.55%). The TGA curve for **2** shows two weight-loss stages: the first starts at 40 °C up to 100 °C, giving a weight loss of about 3.68%, corresponding to the loss of uncoordinated water molecules (calcd. 3.86%); the second step covers from 301 to 486 °C, during which the organic ligands are burned, the weight loss of 88.31% (calcd. 88.53%), the remaining weight corresponds to MnO. The TGA curve of **3** indicates that only one weight loss stage exists in the region of 239–356 °C. The weight loss at this stage is observed to be 91.03%, corresponding to the decomposition of PIP ligand and 1,4-bdc (calcd. 91.22%), the remaining weight corresponds to MnO. The decomposition of complex **4** was similar to that of complex **3**, but showed higher thermal stability. Here a rapid mass loss began at 334 °C and completed by 418 °C, which corresponds to the loss of 86.52% (calcd. 86.21%). For **5**, a slight decrease in mass about 2.17% at 87–110 °C marks the expulsion of water molecule of crystallization. Elimination of the remaining components in **5** began at 230 °C corresponding to the decomposition of the organic ligands, the weight loss of 89.48% (calcd. 89.73%). The TGA trace of complex **6** exhibits two main steps of weight loss, too. The first step started at 154 °C and completed at 177 °C, which corresponds to the release of lattice water molecules. The second step covers from 237 to 333 °C, during which the organic ligands are burned, the weight loss of 87.33% (calcd. 87.47%), the remaining weight corresponds to MnO.

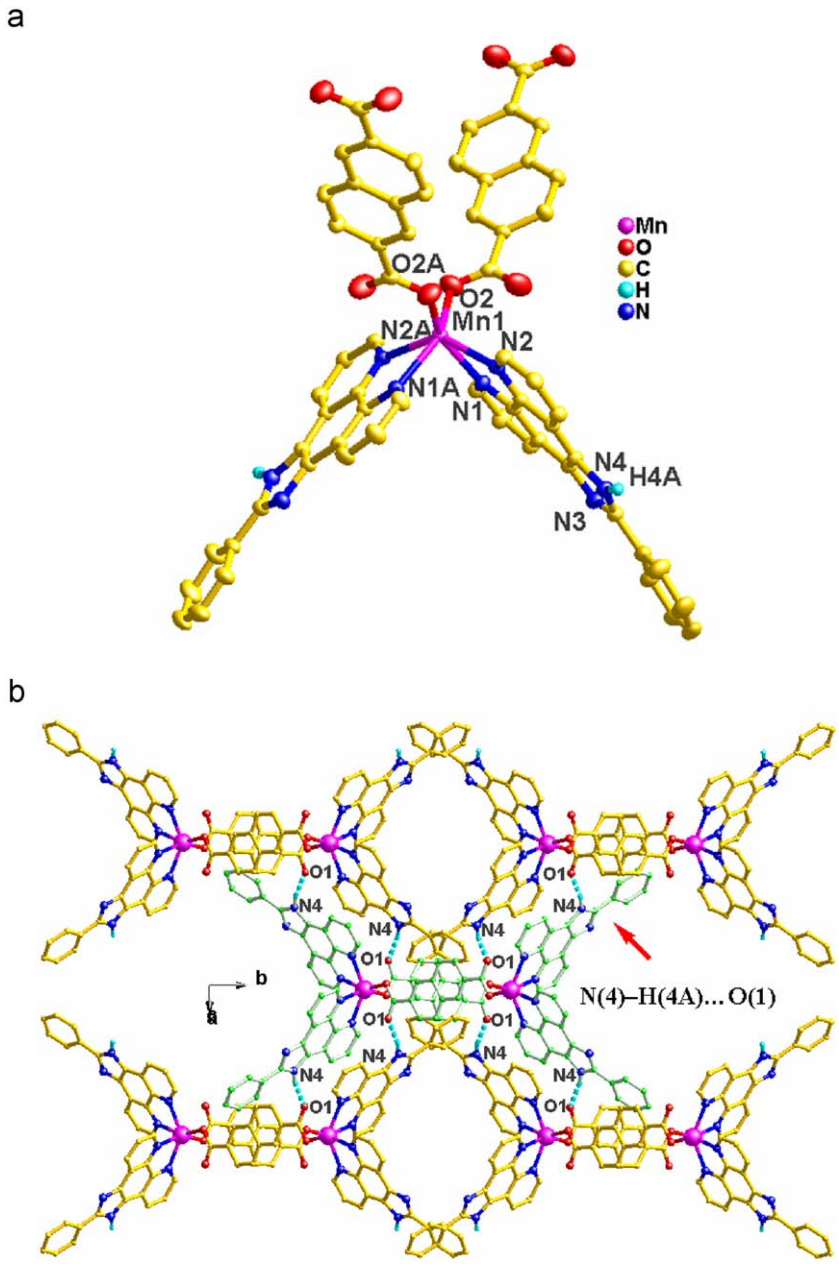

Fig. 5. View of (a) the coordination environment of Mn(II) in **5** (symmetry code: **A**: $-x-1/2, y, -z+1/2$); (b) the 3D supramolecular structure formed by N–H···O weak interactions between 1D zigzag chains in **5**, viewed along the *c*-axis.

3.4. Magnetic property of complex **4**

The magnetic behaviors of **4** in the temperature range 2–300 K are shown as plots of the product $\chi_M T$ versus T and $1/\chi_M$ versus T in Fig. 7. At 300 K, the value of magnetic moments (μ_{eff}), which is determined from the equation $\mu_{eff} = 2.828(\chi_M T)^{1/2}$, is 8.23 μ_B, and slightly smaller than that expected value 10.95 μ_B for the isolated two Mn(II) ions ($S = 5$; $g = 2.0$) [48–50]. The $\chi_M T$ value has little changes before 50 K with the decreasing of temperature. With the continuous decreasing of temperature, the $\chi_M T$ value decreases sharply and reach the minimum value of 1.20 emu K mol^{-1} (3.10 μ_B) at 2 K. The $1/\chi_M$ versus T plot in Fig. 7 displays Curie–Weiss paramagnetic behavior from 30 to 300 K. The best linear fit of $\chi_M{}^{-1}(T)$ data above 30 K yields $C = 8.62$ emu K mol^{-1} and $T = -4.00$ K. The negative constant indicates dominant antiferromagnetic interactions between Mn(II)–Mn(II) through the carboxylic bridge [51,52].

4. Conclusions

In summary, six new Mn(II) complexes were synthesized and structurally characterized. Single crystal structure analysis shows that **1** and **2** possess mononuclear structures, **3**, **4**, and **5** present different 1D chains structures, while **6** is a 2D (4,4) network complex. These results indicate that organic carboxylate anions play an important role in the structure control of Mn(II)

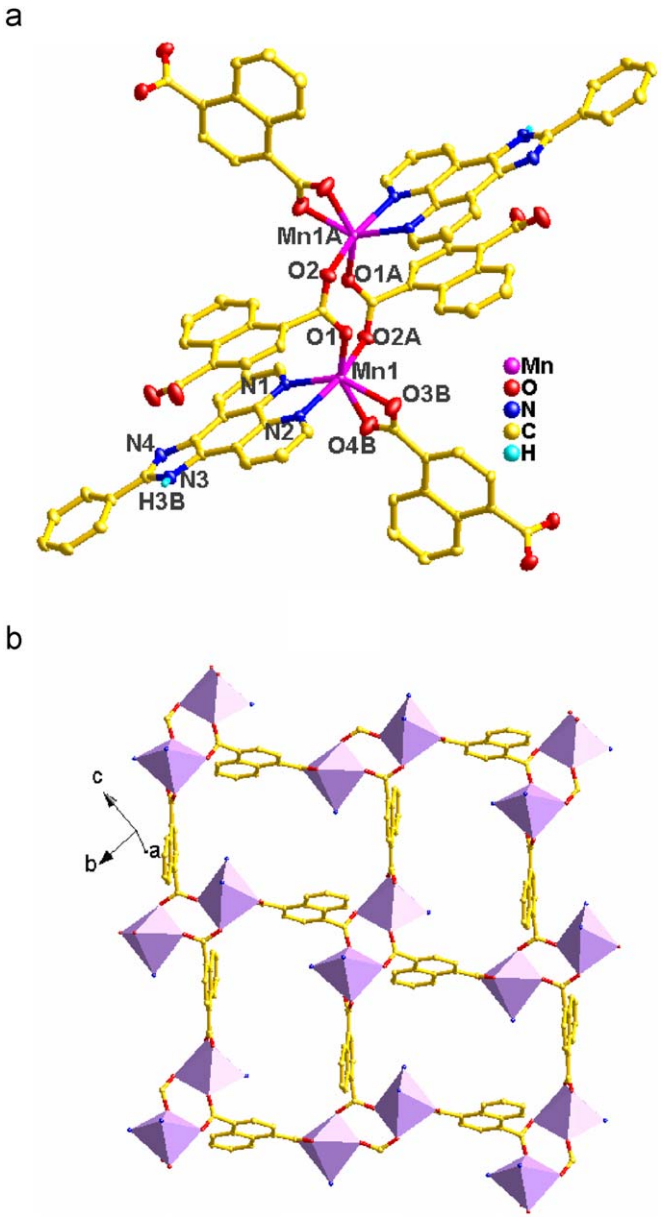

Fig. 6. View of (a) the coordination environment of Mn(II) in **6** (symmetry code: **A**: $-x+1, -y+1, -z+1$; **B**: $x, -y+1/2, z+1/2$); (b) the 2D network of complex **6**.

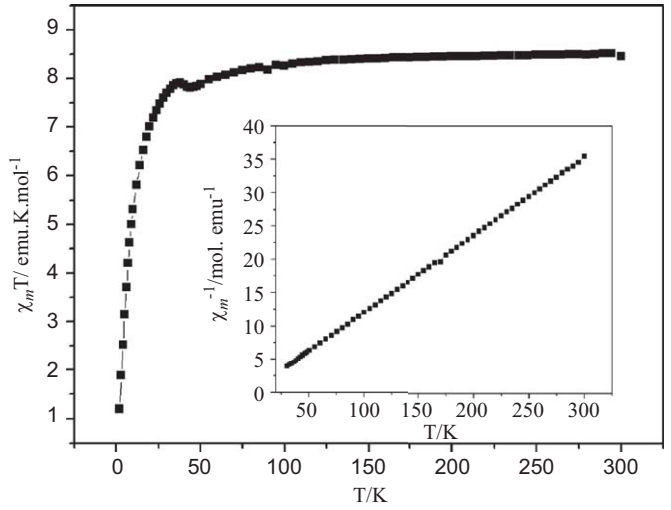

Fig. 7. Plot of $\chi_M T$ versus T for **4**. The insert shows the $1/\chi_M$ versus T for complex **4**.

complexes, which is very significant in the design and syntheses of Mn(II)-based inorganic–organic hybrid materials.

Supporting information available

X-ray crystallographic information files (CIF) for **1–6**, selected bond distances and angles, together with TGA spectra are available free of charge via the Internet at http://pubs.acs.org.

Acknowledgments

This work was supported by the National Natural Science Foundation of China (no. 20871022) and Natural Science Foundation of Liaoning Province (no. 20061073).

Appendix A. Supplementary material

Supplementary data associated with this article can be found in the online version at doi:10.1016/j.jssc.2009.06.031.

References

[1] M. Yuan, F. Zhao, W. Zhang, Z.M. Wang, S. Gao, Inorg. Chem. 46 (2007) 11235.
[2] S.R. Batten, R. Robson, Angew. Chem. Int. Ed. 37 (1998) 1460.
[3] O.M. Yaghi, M. O'Keeffe, N.W. Ockwig, H.K. Chae, M. Eddaoudi, J. Kim, Nature 423 (2003) 705.
[4] S. Kitagawa, R. Kitaura, S. Noro, Angew. Chem. Int. Ed. 43 (2004) 2334.
[5] A.Y. Robin, K.M. Fromm, Coord. Chem. Rev. 250 (2006) 2127.
[6] J.P. Zhang, S.L. Zheng, X.C. Huang, X.M. Chen, Angew. Chem. Int. Ed. 43 (2004) 206.
[7] M.L. Tong, X.M. Chen, S.R. Batten, J. Am. Chem. Soc. 125 (2003) 16170.
[8] C.N.R. Rao, S. Natarajan, R. Vaidhyanathan, Angew. Chem. Int. Ed. 43 (2004) 1466.
[9] G. Ferey, C. Mellot-Draznieks, C. Serre, F. Millange, Acc. Chem. Res. 38 (2005) 217.
[10] I.A. Baburin, V.A. Blatov, L. Carlucci, G. Ciani, D.M. Proserpio, J. Solid State Chem. 178 (2005) 2452.
[11] P.J. Hagrman, D. Hagrman, J. Zubieta, Angew. Chem. Int. Ed. 38 (1999) 2638.
[12] Z.R. Qu, H. Zhao, Y.P. Wang, X.S. Wang, Q. Ye, Y.H. Li, R.G. Xiong, B.F. Abrahams, Z.G. Liu, Z.L. Xue, X.Z. You, Chem. Eur. J. 10 (2004) 53.
[13] X.H. Bu, M.L. Tong, H.C. Chang, S. Kitagawa, S.R. Batten, Angew. Chem. Int. Ed. 43 (2004) 192.
[14] S. Banfi, L. Carlucci, E. Caruso, G. Ciani, D.M. Proserpio, J. Chem. Soc. Dalton Trans. (2002) 2714.
[15] L. Carlucci, G. Ciani, D.M. Proserpio, Angew. Chem. Int. Ed. 34 (1995) 1895.
[16] A.J. Blake, N.R. Champness, P. Hubberstey, W.S. Li, M.A. Withersby, M. Schroder, Coord. Chem. Rev. 183 (1999) 117.
[17] H.L. Zhu, Y.X. Tong, X.M. Chen, J. Chem. Soc. Dalton Trans. (2000) 4182.
[18] M.L. Tong, X.M. Chen, B.H. Ye, S.W. Ng, Inorg. Chem. 37 (1998) 2645.
[19] C.Y. Su, Y.P. Cai, C.L. Chen, F. Lissner, B.S. Kang, W. Kaim, Angew. Chem. Int. Ed. 41 (2002) 3371.
[20] T.L. Honnigar, D.C. MacQuarric, P.D. Rogers, M.J. Zaworotko, Angew. Chem. Int. Ed. 36 (1997) 972.
[21] H. Gudbjarlson, K.M. Poirier, M.J. Zaworotko, J. Am. Chem. Soc. 121 (1999) 2599.
[22] S.Q. Zang, Y. Su, Y.Z. Li, J.G. Lin, X.Y. Duan, Q.J. Meng, S. Gao, Cryst. Eng. Commun. 11 (2009) 122.
[23] R.D. Poulsen, A. Bentien, M. Chevalier, B.B. Iversen, J. Am. Chem. Soc. 127 (2005) 9156.
[24] C.M.R. Juan, B. Lee, Coord. Chem. Rev. 183 (1999) 43.
[25] T.N. Guru Row, Coord. Chem. Rev. 183 (1999) 81.
[26] Z.B. Han, X.N. Cheng, X.M. Chen, Cryst. Growth Des. 5 (2005) 695.
[27] S.S. Kuduva, D.C. Craig, A. Nangia, G.R. Desiraju, J. Am. Chem. Soc. 121 (1999) 1936.
[28] I. Unamuno, J.M. Gutierrez-Zorrilla, A. Luque, P. Roman, L. Lezama, R. Calvo, T. Rojo, Inorg. Chem. 37 (1998) 6452.
[29] J. Yang, J.F. Ma, Y.Y. Liu, J.C. Ma, S.R. Batten, Inorg. Chem. 46 (2007) 6542.
[30] Y.H. Zhao, H.B. Xu, Y.M. Fu, K.Z. Shao, S.Y. Yang, Z.M. Su, X.R. Hao, D.X. Zhu, E.B. Wang, Cryst. Growth Des. 8 (2008) 3566.
[31] L. Ballester, I. Baxter, P.C.M. Duncan, D.M.L. Goodgame, D.A. Grachvogel, D.J. Williams, Polyhedron 17 (1998) 2502.
[32] J. Yang, G.D. Li, J.J. Cao, Q. Yue, G.H. Li, J.S. Chen, Chem. Eur. J. 13 (2007) 3248.
[33] X.L. Wang, Y.F. Bi, H.Y. Lin, G.C. Liu, Cryst. Growth Des. 6 (2007) 1086.

[34] X.L. Wang, Y.F. Bi, G.C. Liu, H.Y. Lin, T.L. Hu, X.H. Bu, Cryst. Eng. Commun. 10 (2008) 349.
[35] X.L. Wang, Y.F. Bi, H.Y. Lin, G.C. Liu, B.K. Chen, J. Organomet. Chem. 692 (2007) 4353.
[36] X.L. Wang, H.Y. Lin, G.C. Liu, H.Y. Zhao, B.K. Chen, J. Organomet. Chem. 693 (2008) 2767.
[37] M.D. Stephenson, M.J. Hardie, Cryst. Growth Des. 6 (2006) 423.
[38] J.H. Liu, X.Z. Ren, H. Xu, Y. Huang, J.Z. Liu, L.N. Ji, Q.L. Zhang, J. Inorg. Biochem. 95 (2003) 194.
[39] O. Kahn, Molecular Magnetism, VCH Publishers, New York, 1993.
[40] G.M. Sheldrick, SHELXS-97, Program for the Solution of Crystal Structure, University of Göttingen, Göttingen, Germany, 1997.
[41] G.M. Sheldrick, SHELXL-97, Program for the Refinement of Crystal Structure, University of Göttingen, Göttingen, Germany, 1997.
[42] D.F. Sun, R. Cao, Y.C. Liang, Q. Shi, W.P. Su, M.-C. Hong, J. Chem. Soc. Dalton Trans. (2001) 2335.
[43] T.K. Maji, W. Kaneko, M. Ohba, S. Kitagawa, Chem. Commun. (2005) 4613.
[44] J. Yang, J.F. Ma, Y.Y. Liu, J.C. Ma, S.R. Batten, Cryst. Growth Des. 9 (2009) 1894.
[45] F.C. Liu, Y.F. Zeng, J.P. Zhao, B.W. Hu, E.C. Sanudo, J. Ribas, X.H. Bu, Inorg. Chem. 46 (2007) 7698.
[46] Z. Wang, V.C. Kravtsov, M.J. Zaworotko, Angew. Chem. Int. Ed. 44 (2005) 2.
[47] A.X. Tian, J. Ying, J. Peng, J.Q. Sha, H.J. Pang, P.P. Zhang, Y. Chen, M. Zhu, Z.M. Su, Cryst. Growth Des. 8 (2008) 3717.
[48] W. Chen, Q. Yue, C. Chen, H.M. Yuang, W. Xu, J.S. Chen, S.N. Wang, Dalton Trans. (2003) 28.
[49] Y.X. Huang, B. Ewaid, W. Schnelle, Y. Prots, R. Kniep, Inorg. Chem. 45 (2006) 7578.
[50] X.T. Zhang, J.M. Dou, D.Q. Wang, Y.X. Zhang, Y. Zhou, R.J. Li, S.S. Yan, Z.H. Ni, J.Z. Jiang, Cryst. Growth Des. 7 (2007) 1699.
[51] J.P. Wang, J.W. Zhao, X.Y. Duan, J.Y. Niu, Cryst. Growth Des. 6 (2006) 507.
[52] J. Lu, E.H. Shen, M. Yuan, Y.G. Li, E.B. Wang, C.W. Hu, L. Xu, J. Peng, Inorg. Chem. 42 (2003) 6956.